Available online at www.sciencedirect.com
SCIENCE DIRECT®
International Journal of Thermal Sciences 44 (2005) 1024–1038
International Journal of Thermal Sciences
www.elsevier.com/locate/ijts

Application of a sensitivity equation method to turbulent flows with heat transfer

E. Colin [a], S. Etienne [a], D. Pelletier [a,*], J. Borggaard [b]

[a] *Département de Génie Mécanique, École Polytechnique de Montréal, Montréal, Québec, H3C 3A7 Canada*
[b] *Interdisciplinary Center for Applied Mathematics, Department of Mathematics, Virginia Tech, Blacksburg, VA 24061-0531, USA*

Received 25 June 2004; received in revised form 10 April 2005; accepted 11 April 2005

Available online 6 June 2005

Abstract

This paper presents a continuous sensitivity equation method (SEM) for incompressible turbulent heat transfer. The k–ε model of turbulence with wall functions is used to model turbulence. Heat transfer is handled using an eddy conductivity. The SEM formulation accounts for complex parameter dependence and is suitable for a wide range of problems. It is applied to turbulent flow over a heated backward facing step and to turbulent flow over a heated flat plate. Several uses of the SEM are demonstrated: fast computation of nearby flows, identification of key parameters controlling the flow, and uncertainty analysis. Sensitivities are used to cascade input data uncertainties through the CFD code to yield uncertainty estimates of the skin friction and Stanton number. The SEM also provides detailed information about the contribution of each parameter to the global uncertainty.

Keywords: Sensitivity equation method; Sensitivity analysis; Turbulent heat transfer; Finite elements; Adaptive remeshing; k–ε model; Wall functions

1. Introduction

CFD has become a common tool of engineering fluid mechanics. With improved algorithms and faster computers the focus is shifting from analyzing a configuration for a given operating condition, to characterizing the behavior of the system at off-design conditions. Inroads have also been achieved in design optimization. However, the design of some systems cannot always easily be cast in the form of an optimization problem. Hence, there is a need for tools to extend the reach of the designer's craft. The engineer must not only know his flow, he must also have an idea of how the flow responds to changes in the design and operation parameters. Finally, most systems operate with uncertain parameters or with parameters know within a given accuracy or uncertainty. Consequently, engineers must assess the effect of input data uncertainty on the response of the system. The sensitivity equation method (SEM) is one of many tools to answer these questions.

This paper focuses on turbulent heat transfer applications of the SEM developed previously by the authors [1]. Turbulence is treated with the k–ε model with wall function and turbulent heat transfer is handled via an eddy diffusivity. We have opted for this model because it is very popular and is available in almost all commercial CFD codes. It is also often the recommended initial approach by software vendors because of its cost-effectiveness (it requires coarser meshes) compared to low Reynolds number models. The SEM for isothermal turbulent flows was demonstrated by Turgeon et al. [2–4]. While sensitivities can be used for design optimization [5,6], they find practical uses in other areas of applications. The paper focuses on these non-optimization uses of the SEM: characterization of thermal systems, identification of key parameters controlling the behavior of the flow, fast evaluation of nearby problems and uncertainty analysis. The latter consist in using sensitivities to cascade input data uncertainty through the CFD code to yield uncertainty estimates of the hydrodynamic and thermal response of the flow.

* Corresponding author.
E-mail address: dominique.pelletier@polymtl.ca (D. Pelletier).

1290-0729/$ – see front matter
doi:10.1016/j.ijthermalsci.2005.04.002

Nomenclature

C_1, C_2, C_μ, σ_k, σ_ε	k–ε model constants
c_p	specific heat
C_f	skin friction coefficient
d	imposed distance to the wall
$\mathbf{f}$	body force
E	roughness parameter
k	turbulence kinetic energy
$\mathcal{K}$	natural logarithm of k
ε	turbulence dissipation rate
$\mathcal{E}$	natural logarithm of ε
$\hat{\mathbf{n}}$, $\hat{\mathbf{t}}$	normal and tangent unit vectors
p	pressure
T	temperature
P	production of turbulence
q	heat flux
q_k, q_ε	turbulence source terms
Re	Reynolds number
St	Stanton number
Pr	Prandtl number
Pr_t	turbulent Prandtl number
s_x	sensitivity of dependent variable x
$\mathbf{u}$	velocity
u, v	velocity components
u_k	velocity scale based on k
u_{**}	friction velocity
x, y	Cartesian coordinates
y	distance to the wall
κ	Kármán constant
μ	viscosity
μ_t	eddy viscosity
λ	conductivity
λ_t	eddy conductivity
ρ	density
τ_w	wall shear stress

Subscripts

e	effective
t	turbulent
w	wall value
x	based on plate length
∞	free-stream value

Superscripts

$'$	sensitivity (derivative)
$+$	dimensionless (wall functions)

The paper begins with the flow equations and boundary equations. This is followed by a presentation of the sensitivity equations and their boundary conditions. Scaled sensitivities are introduced as a convenient tool to compare the effects of different parameters. Application of the SEM to fast evaluation of nearby flows is then discussed. This is followed by a discussion of uncertainty analysis using sensitivity data. The methodology is then demonstrated on two problems: turbulent heat transfer over the backward facing step, and over a heated flat plate. Applications cover sensitivity analysis, identification of key parameters, fast evaluation of nearby flows, and uncertainty analysis. The paper ends with conclusions.

2. Flow equations

2.1. Reynolds-averaged Navier–Stokes equations

The flows of interest are modeled by the time-averaged momentum, continuity and energy equations:

$$\rho\mathbf{u}\cdot\nabla\mathbf{u} = -\nabla p + \mathbf{f} + \nabla\cdot\left[(\mu+\mu_t)\left(\nabla\mathbf{u} + (\nabla\mathbf{u})^{\mathrm{T}}\right)\right] \quad (1)$$

$$\nabla\cdot\mathbf{u} = 0 \quad (2)$$

$$\rho c_p\mathbf{u}\cdot\nabla T = q + \nabla\cdot\left[(\lambda+\lambda_t)\nabla T\right] \quad (3)$$

where ρ is the density, $\mathbf{u}$ is the velocity, p is the pressure, μ is the viscosity, μ_t the eddy viscosity, c_p the specific heat, T the temperature, λ the conductivity and λ_t the eddy conductivity; $\mathbf{f}$ is a body force and q is a heat source.

The eddy viscosity is expressed in terms of two turbulence variables, the turbulence kinetic energy k and its rate of dissipation ε:

$$\mu_t = \rho C_\mu\frac{k^2}{\varepsilon}$$

The eddy conductivity is given by:

$$\lambda_t = \frac{c_p\mu_t}{Pr_t}$$

in which the turbulent Prandtl number Pr_t is equal to unity. The system is closed by using the k–ε model of turbulence [7]. To preserve positivity of the dependent variables, we work with the logarithmic form of these equations [8,9]. This can be viewed as using the following change of dependent variables:

$$\mathcal{K} = \ln(k) \quad \text{and} \quad \mathcal{E} = \ln(\varepsilon).$$

The transport equations for the logarithmic variables become:

$$\rho\mathbf{u}\cdot\nabla\mathcal{K} = \nabla\cdot\left[\left(\mu+\frac{\mu_t}{\sigma_k}\right)\nabla\mathcal{K}\right] + \left(\mu+\frac{\mu_t}{\sigma_k}\right)\nabla\mathcal{K}\cdot\nabla\mathcal{K} + \mu_t e^{-\mathcal{K}}P - \rho^2 C_\mu\frac{e^{\mathcal{K}}}{\mu_t} + q_{\mathcal{K}} \quad (4)$$

$$\rho\mathbf{u}\cdot\nabla\mathcal{E} = \nabla\cdot\left[\left(\mu+\frac{\mu_t}{\sigma_\varepsilon}\right)\nabla\mathcal{E}\right] + \left(\mu+\frac{\mu_t}{\sigma_\varepsilon}\right)\nabla\mathcal{E}\cdot\nabla\mathcal{E} + \rho C_1 C_\mu e^{\mathcal{K}-\mathcal{E}}P - C_2\rho e^{\mathcal{E}-\mathcal{K}} + q_{\mathcal{E}} \quad (5)$$

Table 1
Constants for the k–ε model

C_μ	C_1	C_2	σ_k	σ_ε
0.09	1.44	1.92	1.0	1.3

The production of turbulence P is defined as

$$P = \nabla\mathbf{u} : \left(\nabla\mathbf{u} + (\nabla\mathbf{u})^{\mathrm{T}}\right)$$

The constants C_1, C_2, C_μ, σ_k, and σ_ε are set to the values recommended by Launder and Spalding [7] and are given in Table 1.

Finally, $q_{\mathcal{K}}$ and $q_{\mathcal{E}}$ are user supplied source terms used for code verification by the Method of Manufactured Solutions. See Section 7.1 for details.

2.2. Wall boundary conditions

The standard k–ε turbulence model is not valid when the turbulence Reynolds number is low (i.e., the near-wall region). Wall functions are used to describe the solution near the wall. We use the two-velocity scale wall functions described in Refs. [10,11]. Its universal velocity profile is given by:

$$u^+ = \begin{cases} y^+ & \text{for } y^+ < y_c^+ \\ \frac{1}{\kappa}\ln(Ey^+) & \text{for } y^+ \geqslant y_c^+ \end{cases} \tag{6}$$

where κ is the Kármán constant and E a roughness parameter. For smooth walls we take $\kappa = 0.42$ and $E = 9.0$. The transition point y_c^+ is obtained from the intersection of the two curves, in this case $y_c^+ \approx 11$. The dimensionless distance to the wall y^+ and the dimensionless tangential velocity u^+ are given by:

$$y^+ = \frac{\rho y u_k}{\mu} \tag{7}$$

$$u^+ = \frac{u_t}{u_{**}} \tag{8}$$

where u_t is the tangential velocity and y is the distance normal to the wall.

This wall function involves two velocity scales: u_k, a scale based on the turbulence kinetic energy

$$u_k = C_\mu^{1/4} k^{1/2} \tag{9}$$

where k is taken at the boundary of the computational domain; and u_{**}, a scale based on the friction velocity u_* and defined as

$$(u_*)^2 = u_k u_{**} \tag{10}$$

The boundary conditions for k, ε, and the momentum equations at a distance $y = d$ from the wall are:

$$\frac{\partial k}{\partial n} = 0 \quad \text{or} \quad \left(\mu + \frac{\mu_t}{\sigma_k}\right)\nabla\mathcal{K}\cdot\hat{\mathbf{n}} = 0 \tag{11}$$

$$\varepsilon = \frac{u_k^3}{\kappa d} \quad \text{or} \quad \mathcal{E} = \ln\left(\frac{u_k^3}{\kappa d}\right) \tag{12}$$

$$\mathbf{u}\cdot\hat{\mathbf{n}} = 0 \tag{13}$$

$$\tau_w = \rho u_{**} u_k \tag{14}$$

where $\hat{\mathbf{n}}$ is the normal unit vector. Note that substitution of Eqs. (6)–(9) into Eq. (14) provides a relationship between the wall shear stress τ_w and the velocity u_t (i.e., a mixed or Robin boundary condition).

2.3. Thermal wall function

Boundary conditions for the energy equation are enforced through a temperature wall function. For constant wall heat flux, the boundary condition is:

$$(\lambda + \lambda_t)\frac{\partial T}{\partial n} = q_w \tag{15}$$

The wall temperature is extracted from the wall function with:

$$T_w = T + \frac{q_w T^+}{\rho c_p u_k} \tag{16}$$

For constant wall temperature, an effective heat flux is imposed in the wall function

$$q_w = \frac{\rho c_p C_\mu^{1/4} k_w^{1/2}(T_w - T)}{T^+} \tag{17}$$

where T and k are the temperature and the TKE of the boundary of the computational domain; T_w is the wall temperature and T^+ satisfies the following relations [12]:

$$T^+ = \begin{cases} Pr\, y^+ & \text{for } y^+ < y_1^+ \\ a_2 - \frac{Pr_t}{2a_1(y^+)^2} & \text{for } y_1^+ \leqslant y^+ \leqslant y_2^+ \\ \frac{Pr_t}{\kappa}\ln(y^+) + \beta & \text{for } y_2^+ < y^+ \end{cases} \tag{18}$$

with the following definitions

$$y_1^+ = \frac{10}{Pr^{1/3}}, \qquad y_2^+ = \left(\frac{\kappa}{a_1}\right)^{1/2}$$

$$a_1 = 10^{-3} Pr_t, \qquad a_2 = 15 Pr^{2/3}$$

$$\beta = a_2 - \frac{Pr_t}{2\kappa}\left[1 + \ln\left(\frac{\kappa}{a_1}\right)\right]$$

The Prandtl and turbulent Prandtl numbers are set respectively to 0.7 and 1.

3. Sensitivity equations

3.1. Reynolds-averaged Navier–Stokes equations

The continuous sensitivity equations (CSE) are obtained by implicit differentiation of the flow Eqs. (1)–(3) with respect to a given parameter a. This parameter could be a boundary condition (inflow velocity, wall temperature or heat flux for example), a closure coefficient of the turbulence model, a physical property of the fluid, or a coefficient appearing in the momentum or thermal wall functions. Thus, we consider the variable $\mathbf{u}$ to depend on spatial coordinates and on parameter a. This dependence is denoted as

$\mathbf{u}(\mathbf{x}; a)$. Defining the flow sensitivities as the partial derivatives $\mathbf{s}_u = \frac{\partial \mathbf{u}}{\partial a}$ and $s_T = \frac{\partial T}{\partial a}$, and the total derivatives of the fluid properties and other flow parameters by a ($'$), we obtain

$$\begin{aligned}&\rho'\mathbf{u}\cdot\nabla\mathbf{u} + \rho\mathbf{s}_u\cdot\nabla\mathbf{u} + \rho\mathbf{u}\cdot\nabla\mathbf{s}_u \\ &\quad = -\nabla s_p + \mathbf{f}' + \nabla\cdot\big[(\mu'+\mu_t')\big(\nabla\mathbf{u} + (\nabla\mathbf{u})^{\mathrm{T}}\big) \\ &\qquad + (\mu+\mu_t)\big(\nabla\mathbf{s}_u + (\nabla\mathbf{s}_u)^{\mathrm{T}}\big)\big] \qquad (19)\\ &\nabla\cdot\mathbf{s}_u = 0 \qquad (20)\\ &\rho'\mathbf{u}\cdot\nabla T + \rho\mathbf{s}_u\cdot\nabla T + \rho\mathbf{u}\cdot\nabla s_T \\ &\quad = q' + \nabla\cdot\big[(\lambda'+\lambda_t')\nabla T + (\lambda+\lambda_t)\nabla s_T\big] \qquad (21)\end{aligned}$$

3.2. Turbulence equations

Differentiation of the turbulence transport equations (4) and (5) with respect to parameter a yields the continuous sensitivity equations for $s_{\mathcal{K}}$ and $s_{\mathcal{E}}$:

$$\begin{aligned}&\rho'\mathbf{u}\cdot\nabla\mathcal{K} + \rho\mathbf{s}_u\cdot\nabla\mathcal{K} + \rho\mathbf{u}\cdot\nabla s_{\mathcal{K}} \\ &\quad = \nabla\cdot\left[\left(\mu' + \frac{\mu_t'}{\sigma_k} - \frac{\mu_t\sigma_k'}{\sigma_k^2}\right)\nabla\mathcal{K} + \left(\mu + \frac{\mu_t}{\sigma_k}\right)\nabla s_{\mathcal{K}}\right] \\ &\qquad + \left(\mu' + \frac{\mu_t'}{\sigma_k} - \frac{\mu_t\sigma_k'}{\sigma_k^2}\right)\nabla\mathcal{K}\cdot\nabla\mathcal{K} \\ &\qquad + 2\left(\mu + \frac{\mu_t}{\sigma_k}\right)\nabla\mathcal{K}\cdot\nabla s_{\mathcal{K}} \\ &\qquad + e^{-\mathcal{K}}(\mu_t' P + \mu_t P' - \mu_t P s_{\mathcal{K}}) \\ &\qquad - \rho e^{\mathcal{E}-\mathcal{K}}\left(2\frac{\rho'}{\rho} + \frac{C_\mu'}{C_\mu} + s_{\mathcal{K}} - \frac{\mu_t'}{\mu_t}\right) + q_{\mathcal{K}}' \qquad (22)\end{aligned}$$

and

$$\begin{aligned}&\rho'\mathbf{u}\cdot\nabla\mathcal{E} + \rho\mathbf{s}_u\cdot\nabla\mathcal{E} + \rho\mathbf{u}\cdot\nabla s_{\mathcal{E}} \\ &\quad = \nabla\cdot\left[\left(\mu' + \frac{\mu_t'}{\sigma_\varepsilon} - \frac{\mu_t\sigma_\varepsilon'}{\sigma_\varepsilon^2}\right)\nabla\mathcal{E} + \left(\mu + \frac{\mu_t}{\sigma_\varepsilon}\right)\nabla s_{\mathcal{E}}\right] \\ &\qquad + \left(\mu' + \frac{\mu_t'}{\sigma_\varepsilon} - \frac{\mu_t\sigma_\varepsilon'}{\sigma_\varepsilon^2}\right)\nabla\mathcal{E}\cdot\nabla\mathcal{E} \\ &\qquad + 2\left(\mu + \frac{\mu_t}{\sigma_\varepsilon}\right)\nabla\mathcal{E}\cdot\nabla s_{\mathcal{E}} \\ &\qquad + \rho C_1 C_\mu e^{\mathcal{K}-\mathcal{E}} P\left(\frac{\rho'}{\rho} + \frac{C_1'}{C_1} + \frac{C_\mu'}{C_\mu} + s_{\mathcal{K}} - s_{\mathcal{E}} + \frac{P'}{P}\right) \\ &\qquad - C_2\rho e^{\mathcal{E}-\mathcal{K}}\left(\frac{C_2'}{C_2} + \frac{\rho'}{\rho} + s_{\mathcal{E}} - s_{\mathcal{K}}\right) + q_{\mathcal{E}}' \qquad (23)\end{aligned}$$

where the sensitivity of the production term is

$$P' = 2\nabla\mathbf{s}_u : \big(\nabla\mathbf{u} + (\nabla\mathbf{u})^{\mathrm{T}}\big)$$

and the sensitivity of the eddy viscosity is

$$\begin{aligned}\mu_t' &= \big(\rho' C_\mu + \rho C_\mu'\big)e^{2\mathcal{K}-\mathcal{E}} + \rho C_\mu e^{2\mathcal{K}-\mathcal{E}}(2s_{\mathcal{K}} - s_{\mathcal{E}}) \\ &= \mu_t\left(\frac{\rho'}{\rho} + \frac{C_\mu'}{C_\mu} + 2s_{\mathcal{K}} - s_{\mathcal{E}}\right)\end{aligned}$$

while that of the eddy conductivity is:

$$\lambda_t' = \lambda_t\left(\frac{c_p'}{c_p} + \frac{\mu_t'}{\mu_t} + \frac{Pr_t'}{Pr_t}\right)$$

3.3. Wall boundary conditions

Wall functions for sensitivity equations are obtained by implicit differentiation of wall functions of the flow equations. For value parameters, differentiation is simplified since the normal and tangent vectors have zero derivative with respect to a. Differentiation of the no-penetration condition (13) leads to

$$\mathbf{s}_u\cdot\hat{\mathbf{n}} = 0$$

whereas the sensitivity of the shear stress is given by

$$\tau_w' = \rho' u_k u_{**} + \rho u_k' u_{**} + \rho u_k u_{**}'$$

The sensitivities u_{**}' and u_k' appearing in this expression are obtained by differentiation of Eqs. (8) and (9):

$$\begin{aligned}u_{**}' &= \frac{u_t'}{u^+} - \frac{u_t u^{+\prime}}{u^{+2}} \\ u_k' &= u_k\left(\frac{1}{4}\frac{C_\mu'}{C_\mu} + \frac{1}{2}s_{\mathcal{K}}\right)\end{aligned}$$

where from (6)

$$u^{+\prime} = \begin{cases} y^{+\prime} & \text{for } y^+ < y_c^+ \\ \frac{1}{\kappa}\big(-u^+\kappa' + \frac{E'}{E} + \frac{y^{+\prime}}{y^+}\big) & \text{for } y^+ \geqslant y_c^+ \end{cases}$$

and from (7)

$$y^{+\prime} = y^+\left(\frac{\rho'}{\rho} + \frac{d'}{d} + \frac{u_k'}{u_k} - \frac{\mu'}{\mu}\right)$$

Finally, for the tangential component of velocity

$$u_t = u t_x + v t_y$$

we get

$$u_t' = s_u t_x + s_v t_y.$$

Here we have assumed that $t_x' = t_y' = 0$ because we consider fixed walls. The distance to the wall d may vary because it is as a value parameter in the wall functions.

From Eq. (15), we deduce the following boundary condition for T:

$$(\lambda'+\lambda_t')\frac{\partial T}{\partial n} + (\lambda+\lambda_t)\frac{\partial s_T}{\partial n} = q_w'$$

whereas the sensitivity of the effective heat flux is given by

$$\begin{aligned}q_w' &= \frac{\rho' c_p u_k (T_w - T)}{T^+} + \frac{\rho c_p' u_k (T_w - T)}{T^+} \\ &\quad + \frac{\rho c_p u_k' (T_w - T)}{T^+} + \frac{\rho c_p u_k (T_w' - S_T)}{T^+} \\ &\quad - \frac{\rho c_p u_k (T_w - T) T^{+\prime}}{(T^+)^2}\end{aligned}$$

The sensitivity u'_k is obtained as shown in three next sections. The sensitivity $(T^+)'$ appearing in this expression is obtained by differentiation of Eqs. (18):

$$T^{+\prime} = \begin{cases} Pr\, y^{+\prime} + Pr' y^+ \\ \quad \text{for } y^+ < y_1^+ \\ a'_2 - \frac{Pr_t}{2a_1(y^+)^2}\left(\frac{Pr'}{Pr} - \frac{a'_1}{a_1} - \frac{2y^{+\prime}}{y^+}\right) \\ \quad \text{for } y_1^+ < y^+ < y_2^+ \\ \frac{Pr_t}{\kappa}\left(\frac{Pr'_t}{Pr_t}\ln y^+ - \frac{\kappa'}{\kappa}\ln y^+ + \frac{y^{+\prime}}{y^+}\right) + \beta' \\ \quad \text{for } y_2^+ \leqslant y^+ \end{cases}$$

where

$$y^{+\prime} = y^+\left(\frac{\rho'}{\rho} + \frac{d'}{d} + \frac{u'_k}{u_k} - \frac{\mu'}{\mu}\right)$$

$$Pr' = Pr\left(\frac{c'_p}{c_p} + \frac{\mu'}{\mu} - \frac{\lambda'}{\lambda}\right)$$

and where the constant derivatives are

$$a'_1 = 10^{-3} Pr'_t$$

$$a'_2 = 10 Pr' Pr^{-1/3}$$

$$\beta' = a'_2 - \left(\frac{Pr'_t\kappa - Pr_t\kappa'}{2\kappa^2}\right)\left[1 + \ln\left(\frac{\kappa}{a_1}\right)\right] - \frac{Pr_t a_1}{2\kappa^2}\frac{\kappa' a_1 - \kappa a'_1}{a_1^2}$$

Finally, from Eq. (11) we deduce the following boundary condition for $s_{\mathcal{K}}$ which is well suited to the natural boundary conditions of the finite element formulation:

$$\left[\left(\mu' + \frac{\mu'_t}{\sigma_k} - \frac{\mu_t\sigma'_k}{\sigma_k^2}\right)\nabla\mathcal{K} + \left(\mu + \frac{\mu_t}{\sigma_k}\right)\nabla s_{\mathcal{K}}\right]\cdot\hat{\mathbf{n}} = 0$$

Finally, the boundary condition for $s_{\mathcal{E}}$ is

$$s_{\mathcal{E}} = 3\frac{u'_k}{u_k} - \frac{\kappa'}{\kappa} - \frac{d'}{d}$$

3.4. Scaled sensitivities

Sensitivities are useful to determine the influence of parameter changes on the flow. However, it is difficult to determine this dependence from the raw information such as $\mathbf{s}_u$, s_p, and so on, since nominal parameters values can differ by several orders of magnitude and may have different units. The nominal value of a is the value of a used for the simulation. In a statistical sense it corresponds to the mean value of the parameter a. A solution to this problem is to scale the sensitivity values by the nominal values of its parameter. For parameters a and b, with nominal (mean) values a_0 and b_0, we can then compare the scaled sensitivities:

$$\frac{\partial\mathbf{u}}{\partial a}a_0 \quad \text{and} \quad \frac{\partial\mathbf{u}}{\partial b}b_0 \tag{24}$$

where a_0 and b_0 are the nominal values of a and b respectively. In this manner comparison of scaled sensitivities is more meaningful because both terms have the same units.

4. Implementation

The flow and sensitivity equations are solved by an adaptive finite element method. Element matrices are constructed using a numerical Jacobian technique. Because of the high Reynolds numbers involved in our application, the flows considered are convection dominated. This is why stabilization terms are added to the standard Galerkin formulation: both GLS and SUPG were used.

The accuracy of the solutions is controlled by an adaptive remeshing strategy. In our case, all variables (flow, temperature and sensitivities) are analyzed and contribute to the mesh adaptation. Error estimates are obtained by a local least-squares reconstruction of the solution derivatives [13, 14]. For velocity, temperature, and turbulence variable the error is measured in the H^1 semi-norm, that is the L_2 norm of the derivatives. For temperature this yields:

$$\|T_{\text{ex}} - T_h\|^2 = \int_\Omega (\nabla T_{\text{ex}} - \nabla T_h)\cdot(\nabla T_{\text{ex}} - \nabla T_h)\,\mathrm{d}A \tag{25}$$

where T_{ex} and T_h are the exact and finite element temperature fields. In practice, T_{ex} is not available; it is replaced by a local least-squares reconstruction of the derivatives [13,14]. For velocity, the error is measured in the strain rate tensor

$$\|U_{\text{ex}} - U_h\|^2 = \int_\Omega (\gamma_{\text{ex}} - \gamma_h) : (\gamma_{\text{ex}} - \gamma_h)\,\mathrm{d}A \tag{26}$$

with

$$\gamma = \frac{1}{2}\left[\nabla\mathbf{u} + (\nabla\mathbf{u})^{\mathrm{T}}\right] \tag{27}$$

A pressure estimate is obtained by projecting the pressure itself. Turbulence variable error estimates are computed in a manner similar to that presented for temperature. The interested reader can find more details in Turgeon et al. [2].

5. Uncertainty analysis

Uncertainty may be viewed as a possible perturbation of a given quantity around its nominal value. The quantity of interest is thus allowed to vary within some limits. Furthermore, changes in input data cause changes in the system response. As an example, consider the horizontal component of the velocity u in a fluid flow. Also, assume that this velocity distribution depends on some parameters $\mathbf{a} = (a_1, a_2, \ldots, a_n)$ describing geometry, boundary conditions, fluid properties, or flow model. If $\mathbf{a}$ is perturbed by $\Delta\mathbf{a}$, the velocity at a point (x, y) may be approximated using a first order Taylor series expansion,

$$u(x, y; \mathbf{a} + \Delta\mathbf{a}) = u(x, y; \mathbf{a}) + \sum_{i=1}^{n}\frac{\partial u}{\partial a_i}(x, y; \mathbf{a})\Delta a_i$$

where we have assumed that $\Delta\mathbf{a}$ is small so that higher order terms may be neglected. The velocity change is thus

$$u(x, y; \mathbf{a} + \Delta\mathbf{a}) - u(x, y; \mathbf{a}) = \sum_{i=1}^{n} \frac{\partial u}{\partial a_i}(x, y; \mathbf{a})\Delta a_i$$

We now look for the propagation of uncertainty from $\mathbf{a}$ to u. If $\Delta\mathbf{a}$ is the uncertainty on $\mathbf{a}$, that is, $\mathbf{a}$ lies somewhere in the interval $\mathbf{a} \pm \Delta\mathbf{a}$. The maximum possible change of u, i.e., its uncertainty Δu, is obtained when the components of $\mathbf{a}$ reach their maximum or minimum values, so that they all work together in the same direction: increasing (or reducing) u. Mathematically, the following inequality holds:

$$\left|u(x, y; \mathbf{a} + \Delta\mathbf{a}) - u(x, y; \mathbf{a})\right| \leqslant \sum_{i=1}^{n} \left| \frac{\partial u}{\partial a_i}(x, y; \mathbf{a})\Delta a_i \right|$$

This expresses exactly what we need. The uncertainty on u corresponds to the "worst case" scenario where velocity changes due to each disturbances Δa_i add up. Thus, we approximate the velocity uncertainty due to Δa_i

$$|\Delta u| \approx \sum_{i=1}^{n} \left| \frac{\partial u}{\partial a_i}(x, y; \mathbf{a}) \right| |\Delta a_i| \tag{28}$$

The preceding development is valid for a single parameter or a set of discrete parameters. In practice, another situation may arise: the uncertainty is distributed. For example, one might be interested in accounting for non-uniformities in a nominally uniform wind tunnel inflow. Such a velocity profile is not constant but exhibits small but measurable *local* disturbances. The uncertainty is best represented by a random variable of space. The velocity profile, and thus its deviation to the nominal profile, are shaped and not defined by a single parameter. The present methodology can still be applied if we can find a parameterization of this shape with uncertainties on the individual parameters. Uncertainties taking the form of numerous localized random variables that may be correlated, can probably be better treated by the stochastic finite element method [15,16]. However, this is beyond the scope of the present paper. The SEM is appropriate for cascading uncertainties in discrete parameter for which the uncertainty is small with respect the mean, while the stochastic FEM is designed to treat uncertainties in the form of random field variables. We restrict our study to uncertainty associated to discrete parameters.

Notice that we can also define an RMS uncertainty by:

$$|\Delta u| \approx \sqrt{\sum_{i=1}^{n} \left| \frac{\partial u}{\partial a_i}(x, y; \mathbf{a}) \right|^2 \Delta a_i^2} \tag{29}$$

This expression provides a smaller uncertainty estimate than that of Eq. (28). Our experience shows that the two estimates behave in a similar manner. Indeed, they are equivalent if there is only one parameter with uncertainty. Hence, results are only presented for the more pessimistic estimate (28).

6. Fast evaluation of nearby flows

The Taylor series expansion can also be used to obtain inexpensive evaluation of solutions at nearby parameter values. This is a very cost effective approach for small changes in the parameter vector $\mathbf{a}$. If we are very close to the baseline solution, we can assume that a first order Taylor series expansion is sufficient and that higher order terms may be neglected. For a single parameter we have:

$$u(x, y; a + \Delta a) = u(x, y; a) + \frac{\partial u}{\partial a}(x, y; a)\Delta a \tag{30}$$

As an example, consider again the horizontal component of the velocity u in a fluid flow. If Δa is small, the above expression provides a good estimate of $u(x, y; a + \Delta a)$ without resorting to a second costly CFD analysis. If a reanalysis yields a value of u close to its Taylor series estimate, then one may conclude that u depends nearly linearly on a. In this case the Taylor series can be used safely for larger perturbations of a. Moreover, the magnitude of the term $\frac{\partial u}{\partial a}(x, y; a)\Delta a$ is an indication of the importance of parameter a on the behavior of the system. A large value indicates a parameter with significant importance while a small value reveals that the influence of the parameter can probably be neglected. These observations extend readily to the case where multiple parameters are considered.

If one performs two flow and sensitivity computations for two distinct values, a_1 and a_2, of parameter a, one can use cubic Hermite polynomials to approximate the flow response of values of a in the interval $[a_1, a_2]$:

$$u(x, y, t) = u(x, y, a_1)\psi_1(\xi) + \frac{\partial u}{\partial a}(x, y; a_1)\psi_2(\xi) + u(x, y, a_2)\psi_3(\xi) + \frac{\partial u}{\partial a}(x, y; a_2)\psi_4(\xi) \tag{31}$$

with

$$\psi_1(\xi) = \frac{1}{4}(1 - \xi)^2(2 + \xi)$$

$$\psi_2(\xi) = \frac{h}{8}\left(1 - \xi^2\right)(1 - \xi)$$

$$\psi_3(\xi) = \frac{1}{4}(1 + \xi)^2(2 - \xi)$$

$$\psi_4(\xi) = \frac{h}{8}\left(-1 + \xi^2\right)(1 + \xi)$$

$$h = a_2 - a_1$$

$$\xi = -1 + 2\left(\frac{t - a_1}{a_2 - a_1}\right)$$

In, general, this expression yields greater accuracy than a linear Taylor series (30). Of course improved accuracy is achieved at a greater computational cost since the Hermite approach requires two flow solutions while the linear Taylor series requires only one. In both approaches mesh adaption controls numerical accuracy. Hermite polynomials usually provide reliable nearby flows on a wider interval than linear Taylor series because the polynomial uses additional information about the flow dependence on the parameter a (i.e.,

two flows and two sensitivity solutions versus one flow and one sensitivity solution). Comparison of Hermite and linear Taylor estimates of u provide additional clues on the linearity of the relation between u and a. For clarity and simplicity we restrict our demonstration of fast nearby flow evaluation to a single parameter. Examples of multiple parameter extrapolation may be found in our previous work. See Turgeon et al. [2,17,18] for details.

7. Numerical results

We begin with a verification example involving a free shear layer with a closed form solution. A grid convergence study is performed to assess the accuracy of the sensitivity solutions as well as the performance of the error estimator.

This is followed by numerical results for two applications: turbulent heat transfer over a backward facing step, and flow over a heated flat plate. The first example is a popular test case since it covers many important turbulent flow phenomena such as separation, recirculation, reattachment and the development of a boundary layer downstream of the reattachment point. Predictions of the Stanton number are compared to measurements. Sensitivity information is used to identify which parameters of the turbulence model have the most influence on the hydrodynamic and thermal behavior of the flow. Input parameter uncertainty is cascaded through the CFD code to yield uncertainty estimates of the skin friction coefficient and Stanton number. Sensitivity information is also used to determine which parameter contributes most significantly to the output uncertainty The second example, turbulent heat transfer on a flat plate, illustrates fast evaluation of nearby flows using linear Taylor series and Hermite polynomials. Uncertainty analysis is also performed. In both examples the parameters considered are the closure coefficients of the k–ε model of turbulence, the coefficients appearing in the wall function and those appearing in the energy equation.

7.1. Verification: A shear layer

We will first verify the correct implementation of the proposed formulation, using the Method of Manufactured Solution proposed by Roache [19]. We use the following expressions as a solution:

$$
\begin{aligned}
U &= \frac{U_1+U_2}{2} - \frac{U_1-U_2}{2}\operatorname{erf}(\eta)\\
V &= \frac{U_1-U_2}{2}\frac{1}{\sigma\sqrt{\pi}}B\\
T &= \frac{T_1+T_2}{2} - \frac{T_1-T_2}{2}\operatorname{erf}(\eta)\\
p &= 0\\
k &= k_0(c_k+B)\\
\varepsilon &= \frac{\varepsilon_0}{x}(c_k+B)\\
\mu_T &= \mu_{T_0}x(c_k+B)
\end{aligned}
\tag{32}
$$

where

$$
\begin{aligned}
&\eta = \frac{\sigma y}{x}, \qquad B = e^{-\eta^2}\\
&U_1 = 1, \qquad U_2 = 0.3\\
&T_1 = 0.3, \qquad T_2 = 1\\
&\sigma = 13.5, \qquad \rho = 1.0\\
&C_\mu = 0.09, \qquad \mu = 10^{-4}\\
&c_k = \frac{10^{-4}}{k_0}, \qquad \mu_{T_0} = \frac{343}{250000}\rho U_1\\
&k_0 = \frac{343}{75000}U_1(U_1-U_2)\frac{\sigma}{\sqrt{\pi}}\\
&\varepsilon_0 = \frac{343}{22500}C_\mu U_1(U_1-U_2)^2\frac{\sigma^2}{\pi}
\end{aligned}
\tag{33}
$$

They become a proper solution to the Reynolds-averaged equations by defining the appropriate forcing functions $\mathbf{f}$, q, $q_{\mathcal{K}}$ and $q_{\mathcal{E}}$. See Colin for details [20]. Analytical expressions for the sensitivities are obtained by differentiation of the above expressions with respect to parameters of interest. The appropriate source terms in the sensitivity equations are obtained by differentiation of the source terms in Eqs. (1), (3)–(5).

This flow mimics a thermal free shear layer. It is solved over the domain $[100, -75] \times [300, 75]$. Dirichlet boundary conditions are evaluated using expressions (32) and applied everywhere, except on a portion of the bottom boundary, where a zero normal traction is specified to ensure that mass is conserved. Following Turgeon et al. [21], computations are performed using a GLS stabilized finite element scheme for all equations (momentum, continuity, energy, turbulence) including the sensitivity equations. The adaptive remeshing strategy is set to reduce the global error by a factor of 2 at each adaptive cycle. All dependent variables and their sensitivities contribute to mesh refinement.

Fig. 1 illustrates the adaptive grid convergence of the flow and temperature sensitivities with respect to U_1 and T_1. The norm of the global error (i.e., over the domain) decreases at each cycle of mesh adaptation indicating that grid convergence is occurring. Notice also that agreement between the error estimates and the true errors improves with mesh adaptation. The estimators exhibit asymptotic exactness with grid refinement. As expected, excellent accuracy improvements are observed. Error trajectories, for all variables, exhibit a slope of 1. Because the number of nodes in the mesh listed on the horizontal axis is proportional to $1/h^2$, the scheme is second order accurate in the derivatives. This verifies the performance and accuracy of the solver and error estimators in the sense of Roache [19].

7.2. A heated backward facing step

The first application is the flow over a heated backward facing step, studied experimentally by Vogel et al. [22]. This seems to be the only experimental fork on turbulent forced

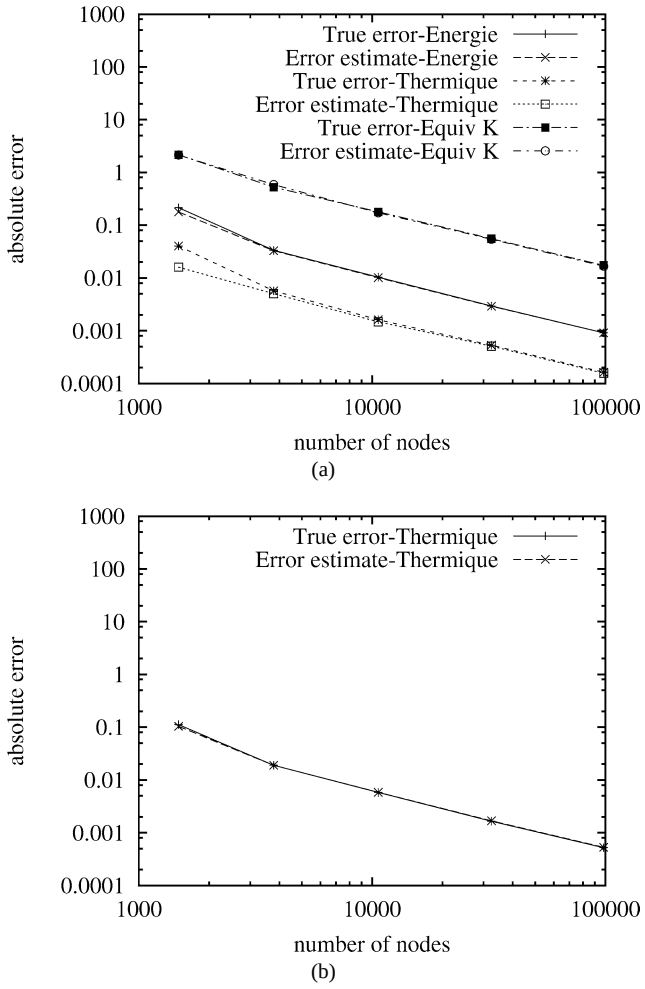

Fig. 1. Verification: Grid convergence of sensitivities. (a) Parameter U_1; (b) Parameter T_1.

convection heat transfer. There exist recent experimental work on turbulent mixed and natural convection [23–25]. However, this is an entirely different flow regime that is beyond the scope of the present paper.

Fig. 2(a) shows the geometry and boundary conditions used in the simulations. For the present case, the Reynolds number is $Re = 28\,000$. Constant dimensionless Dirichlet boundary conditions are applied at the inlet: $u = 1$, $v = 0$, $k = 0.005$, and $\varepsilon = 0.01$; only the temperature is set free. At the outlet, the normal stress, v and the normal derivatives of k and ε are set to zero. Two velocity scale wall functions are used on solid walls with the wall distance d given as follows: $d = 0.08$ on the upstream horizontal surface, $d = 0.1$ on the step face, $d = 0.05$ on the bottom wall, and $d = 0.1$ on the top wall. The heat flux along the bottom wall q_w is set to one, and the other walls are considered adiabatic.

Eleven parameters are considered in the sensitivity analysis: the 5 closure coefficients of the k–ε model of turbulence (C_μ, C_1, C_2, σ_k and σ_e); 3 thermal coefficients (c_p, λ and q_w) and 3 wall function coefficients (d, κ and E). This illustrates the power of the approach. It also shows that sensitivity analysis generates large data sets, in this case the equivalent of 12 flow solutions: the flow itself ($u, v, p, T, k, \varepsilon$) plus 11 sensitivity solution field, each counting 6 variables ($s_u, s_v, s_p, s_T, s_k, s_\varepsilon$).

Fig. 2(b) shows the final adapted mesh obtained after 4 cycles of adaptation. It contains 75 000 nodes and reflects grid adaptation to all flow and sensitivity variables. A high level of refinement exists near the corner of the expansion, in the shear layer and near the top and bottom walls. These zones correspond to regions of rapid changes in the solution and its sensitivities. The refinement on the bottom wall is due to the important gradients of u and T.

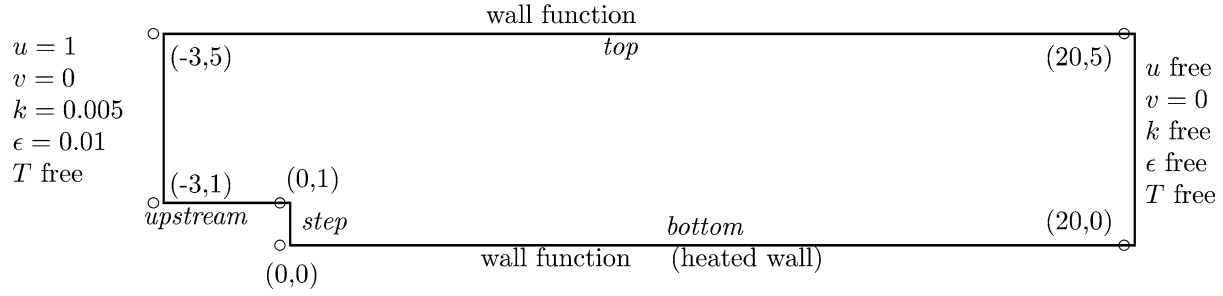

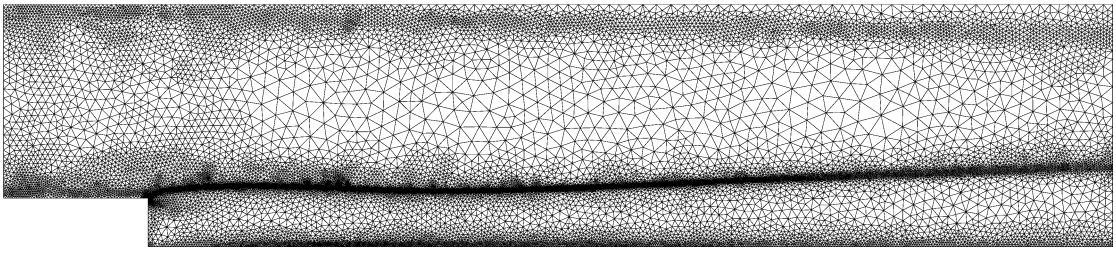

Fig. 2. Backward facing step. (a) Domain definition. (b) Final mesh.

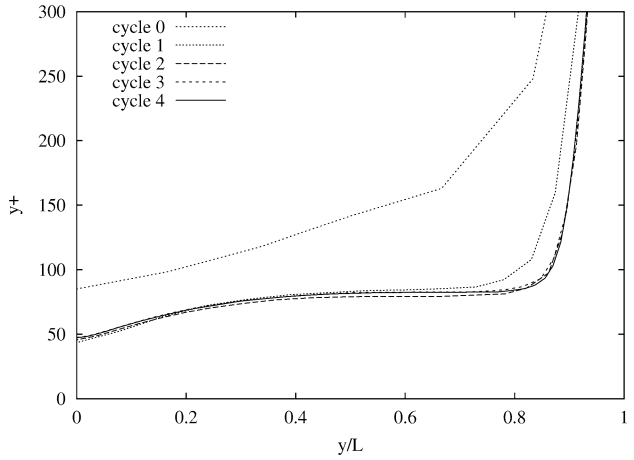

(a)

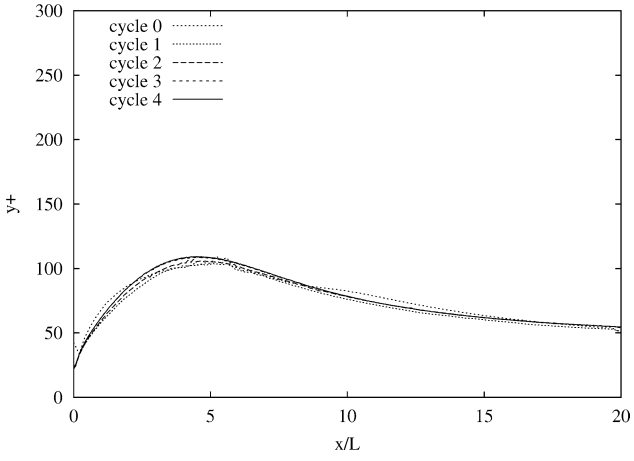

(b)

Fig. 3. Backward facing step: Grid convergence of y^+ along walls. (a) Step face; (b) Bottom wall.

When wall functions are used, one must verify that the specified distance to the solid surface d results in a valid value of d^+ expressed in wall units: $d^+ = \frac{\rho d u_k}{\mu}$ (i.e., Eq. (7)). This value, extracted from a grid converged solution must lie in the interval $[30, 300]$. Fig. 3 shows the convergence and the distribution of y^+ along the step face and the bottom wall. As can be seen, mesh adaptation results in distributions that are well grid converged. See Colin [26] for more details.

The phenomena of interest occur on the bottom wall or near it: stagnation point, boundary layers, recirculation zone etc... They all affect wall shear stress and heat transfer rates which are best presented in the form of the skin friction coefficient C_f and the Stanton number St. Here we use sensitivity information to provide uncertainty estimates of these outputs to perform rigorous comparisons with the experimental measurements of Vogel et al. [22].

For our purpose, the friction coefficient and the Stanton number are defined by:

$$C_f = \frac{\tau}{\frac{1}{2}\rho U_r^2}$$

$$St = \frac{q_w x}{\lambda(T_w - T_r)Re_x Pr}$$

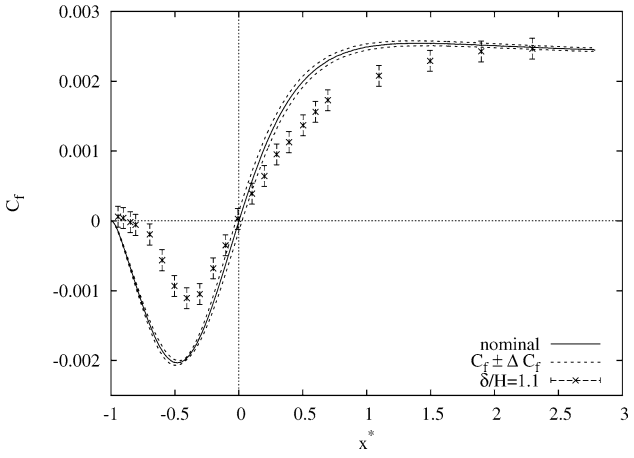

Fig. 4. Backward facing step: Distribution of C_f.

Table 2
Backward facing step: Assumed uncertainties

ΔC_μ	ΔC_1	ΔC_2	$\Delta\sigma_k$	$\Delta\sigma_e$
0.005	0.005	0.005	0.05	0.05
Δc_p	$\Delta\lambda$	Δd	$\Delta\kappa$	ΔE
0.05	5×10^{-6}	0.005	0.005	0.05

From a practical point of view, we compute them using the finite element data and the wall function expressions as follows:

$$C_f = \frac{\rho\kappa u_t u_k}{\ln(Ey^+)}$$

$$St = \frac{q_w}{\rho c_p \widetilde{U}_r (T - T_r) + (\frac{q_w \widetilde{U}_r}{u_k})T^+}$$

This approach yields more accurate values than would be obtained from differentiation of the finite element solution to estimate τ and q_w. In these expressions, U_r is a reference velocity taken as the mean velocity at the inlet and T_r is a reference temperature equal to the inlet temperature.

It is at best a difficult task to assess the uncertainty of the closure and wall function coefficients as no information is available. A reasonable assumption is to consider that these coefficients are accurate to within half a unit of the rightmost digit. Table 2 summarizes the uncertainties used in the present analysis. Note that the actual "accuracy" is probably lower than that provided in the table.

We now illustrate how sensitivity information is used to obtain uncertainty estimates of the flow response. Fig. 4 presents the prediction of the friction coefficient C_f on the bottom wall. This plot includes uncertainty bands due to uncertainties in the turbulence closure coefficient listed in Table 2. The solid line represents the predictions at the nominal values of the parameters while the dashed lines represent the uncertainty intervals determined by Eq. (28). Vogel et al. report an absolute uncertainty in the measurements of 0.00015 (5% of the maximum measured value) [22]. This information is included in the plot for completeness and makes comparison between predictions and measurements a more

rigorous exercise. The results are plotted against the non-dimensional coordinate x^* defined by:

$$x^* = \frac{x - x_r}{x_r} \tag{34}$$

where x_r is the reattachment length. This length and its accuracy will not be discussed in this article; details of its calculation have been discussed by Turgeon et al. [4]. In the present case, we found:

$$x_r = 5.28 \pm 0.02$$

Clearly, predictions are poor, even if we consider the uncertainties. In general, the numerical and experimental uncertainty bands do not overlap. Thus uncertainties in the closure coefficients do not explain the differences between numerical results and experimental measurements. The most likely explanation for the observed discrepancies are the deficiencies in the k–ε model of turbulence as explained by Launder [27]. Another possible source of the discrepancy could be the different thicknesses of the boundary layer at the separation corner point. It is difficult to determine which cause contributes the most to the observed discrepancies. The uncertainty estimates provide little insight in this respect, as their magnitude depends on that of the sensitivities and the assumed parameter uncertainties. The predicted uncertainty bands do not depend on the measurements or their uncertainties; they reflect the effect of our incomplete knowledge of the input parameters on the solution of the Reynolds-averaged Navier–Stokes and k–ε equations. In our case, the thickness of the boundary layer at the separation point is about, $\delta/H = 0.4$, in agreement with the results of Ignat et al. [11]. However, experimental data for skin friction is only available for $\delta/H = 1.1$. Thus comparing predictions for $\delta/H = 0.4$ to measurements taken for $\delta/H = 1.1$ might constitute an unfair comparison and could explain some of the discrepancies. Nonetheless, similar trends are observed: negative values of C_f before the reattachment point followed by positive values downstream of x^*. The small uncertainty on the prediction of C_f was expected due to the small size of both the sensitivities and the associated uncertainties in the closure coefficients.

Using the available sensitivity information, it is possible to identify dominant parameters controlling the flow and to determine which parameter has the most significant contribution to the skin friction uncertainty estimate. Fig. 5(a) compares the scaled sensitivities (see Eq. (24)) with respect to the turbulence closure coefficients. As can be seen, C_1 and C_2 have the most significant influence on the friction coefficient. Moreover, they seem to have a very similar effect, but with opposite signs. Scaled sensitivities cannot be used directly in Eq. (28) to assess individual contributions to the total uncertainty. An expression for the uncertainty using scaled sensitivities can be obtained from Eq. (28) by multiplying and dividing each term by the nominal value of each parameter:

$$|\Delta u| \approx \sum_{i=1}^{n} \left| \frac{\partial u}{\partial a_i} a_{i0} \right| \left| \frac{\Delta a_i}{a_{i0}} \right| \tag{35}$$

Notice now, that the relative uncertainties of each parameter enter in the expression. Hence, the parameter contributing the most to the uncertainty will be characterized by the largest absolute value of its scaled sensitivity multiplied by its relative uncertainty. For completeness the relative uncertainties for the turbulence closure coefficients are given in Table 3.

Fig. 5(b) shows the contribution of each parameter to the global uncertainty. As can be seen, C_μ is the main contributor to the skin friction uncertainty. While the scaled sensitivity of C_f with respect to C_μ is smaller than those of C_f

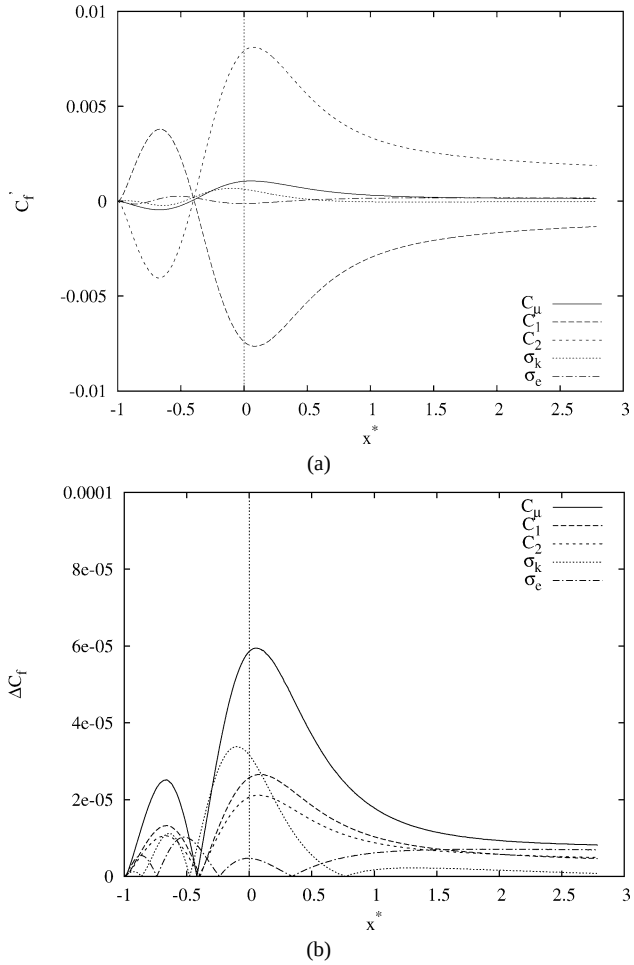

Fig. 5. Backward facing step: Sensitivities and uncertainties in C_f. (a) Scaled sensitivities of C_f; (b) Contributions to C_f uncertainty.

Table 3
Relative uncertainties of closure coefficients

$\frac{\Delta C_\mu}{C_\mu}$	$\frac{\Delta C_1}{C_1}$	$\frac{\Delta C_2}{C_2}$	$\frac{\Delta \sigma_k}{\sigma_k}$	$\frac{\Delta \sigma_e}{\sigma_e}$
5.5%	0.35%	0.26%	5.0%	3.8%

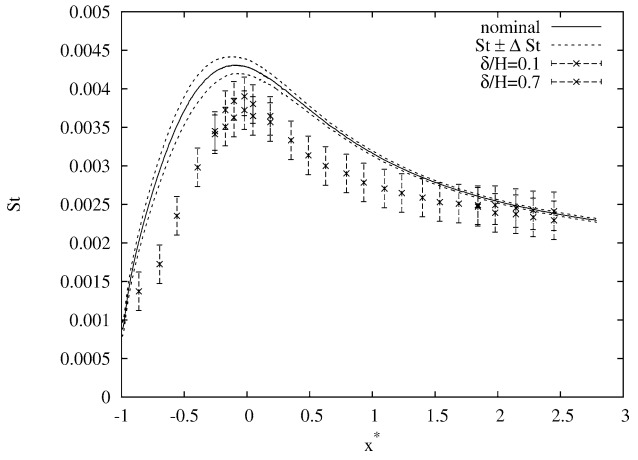

Fig. 6. Backward facing step: Distribution of St.

with respect to C_1 and C_2, the relative uncertainty on C_μ is much larger than the others, conferring to C_μ a dominant contribution to the skin friction uncertainty.

Uncertainty analysis with respect to the closure coefficients is also performed for the Stanton number. Fig. 6 presents its distribution on the bottom wall. In our computations, the thickness of the boundary layer at the separation point is $\delta/H = 0.4$. For comparison we use experimental data collected for $\delta/H = 0.19$ and $\delta/H = 0.7$. These data are given with an experimental uncertainty equal to 0.00025, or 6% of the maximum measured value. The agreement between predictions and measurements is better for the Stanton number than for the skin friction coefficient. The maximum occurs at $x^* = 0$, as expected, and the observed discrepancy is on the order of 11%. The predicted and measured uncertainty intervals do not overlap. Hence, we conclude that uncertainties in the closure coefficients do not explain the observed differences. The k–ε model is not very good for this problem as it has proved to be for other flows [28,29] for which predictions were in better agreement with measurements. In fact, the agreement is at best fair to good, depending on the application needs. Again, the important point is that uncertainties are used to assess the quality, accuracy and reliability of CFD predictions. Their use also ensures that such comparisons are performed on a rigorous basis.

Fig. 7 presents the contributions of individual parameters to the uncertainty in the Stanton number using uncertainty data from Table 2. Sensitivity computations and uncertainty analysis are performed for three groups of parameters: the turbulence closure coefficients ($C_\mu, C_1, C_2, \sigma_K, \sigma_\varepsilon$), the parameter appearing in the hydrodynamic wall function (κ, E, d), and those of the thermal wall function (c_P, λ, q_w). Separate simulations were performed for each group of parameters. Here again, C_μ is the dominant contributor among the closure coefficients. For the hydrodynamic wall function, the Karman constant is responsible for most of the uncertainty except for x^* between -1 and -0.5 where d has the dominant contributor to the uncertainty. The contribution of the roughness parameter to the uncertainty of the Stanton

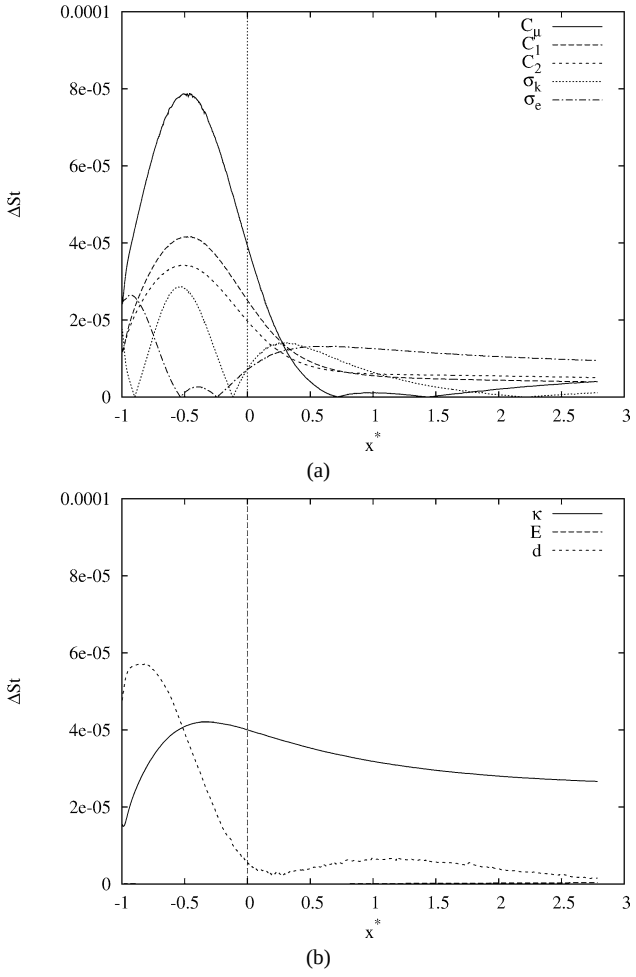

Fig. 7. Backward facing step: Individual contributions to uncertainty of St. (a) Turbulence closure coefficients; (b) Wall function coefficients.

number is so small that it does not show on the plot. For all practical purposes, one can assume that it has no influence on the Stanton number. Finally, among the parameters of the thermal wall function, the specific heat c_p is responsible for most of the uncertainty. The thermal conductivity λ has a much smaller contribution while the applied heat flux q_w has a zero contribution because the sensitivity of the Stanton number with respect to q_w is zero:

$$\frac{\partial St}{\partial q_w} = 0$$

due to the linearity of the heat equation. Thus a change in q_w leaves the dimensionless heat transfer coefficient St unchanged.

This discussion would not be complete without a grid convergence study. Fig. 8 presents the grid convergence of St and that of a typical scaled sensitivity $\lambda\frac{\partial St}{\partial \lambda}$. These quantities are correctly grid converged for the last cycle. Turgeon et al. [4] observed similar trends for an isothermal backward facing step.

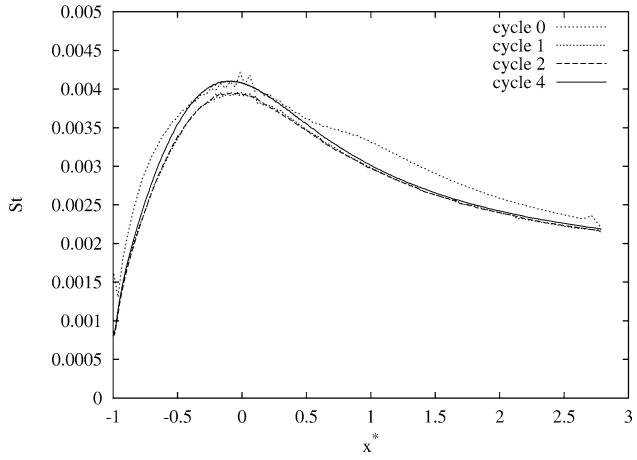

(a)

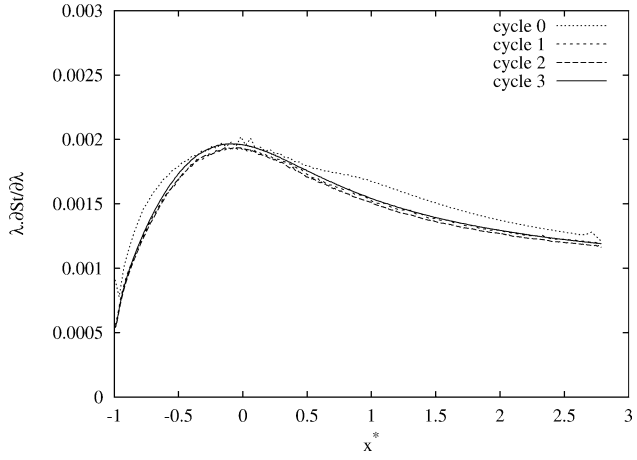

(b)

Fig. 8. Backward facing step: Grid convergence of *St* and $\lambda\frac{\partial St}{\partial\lambda}$. (a) *St*; (b) $\lambda\frac{\partial St}{\partial\lambda}$.

7.3. A heated flat plate

The second application focuses on sensitivity and uncertainty analysis of a developing turbulent boundary layer over a heated flat plate at $Re = 2 \times 10^6$. Preliminary results were presented in a previous paper [1] discussing the general SEM turbulent heat transfer. The domain, its geometry, and a complete description of the boundary conditions are shown in Fig. 9(a).

The plate has a finite thickness and a rounded leading edge. The domain extends to one plate length L upstream and $0.3L$ upwards of the plate. Dimensionless boundary conditions are applied at the inlet: $u = 1$, $v = 0$, $k = 1.0 \times 10^{-6}$ and $\varepsilon = 1.8 \times 10^{-8}$. The parameter d in the wall function is set to $0.00095L$. Fig. 9(b) illustrates the final mesh obtained with the adaptive methodology.

We consider the effects of 10 parameters on the uncertainty of the Stanton number predictions: the 5 closure coefficients of the k–ε model of turbulence (C_μ, C_1, C_2, σ_k and σ_e), 2 thermal coefficients (c_p, λ) and 3 wall function coefficients (d, κ and E).

Fig. 10 compares the prediction of *St* with two accepted correlations:

$$St = \frac{0.0287\widetilde{U}_\infty^{1.8}}{Pr^{0.4}Re_x^{0.2}} \quad \text{(Kays and Crawford [30])}$$

$$St = 0.2275\widetilde{U}_\infty^{2}\left[\ln(0.06Re_x)\right]^{-2} \quad \text{(Pethukov in [30])}$$

An uncertainty band (due to uncertainties in the wall function parameters) is added to the finite element predictions using the approach described previously. Globally, the agreement between predictions and correlations is good. The general trend is a slight under-prediction except near the leading edge. However, the uncertainty band is too narrow to account for the observed discrepancies between predictions and correlations. Again, this mean that the k–ε model appears not to be the best model for predicting the Stanton number for

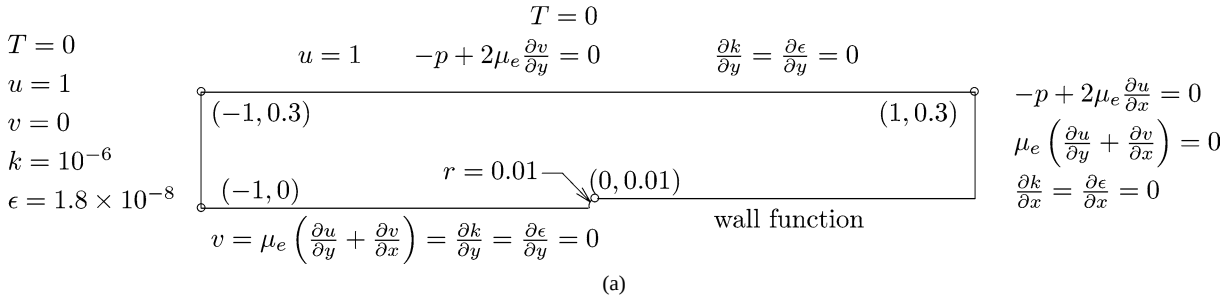

(a)

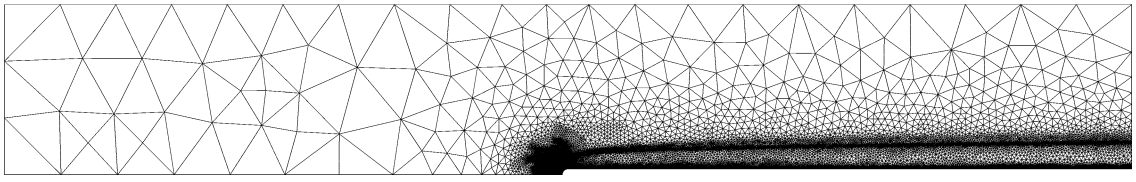

(b)

Fig. 9. Heated flat plate. (a) Domain definition; (b) Final mesh.

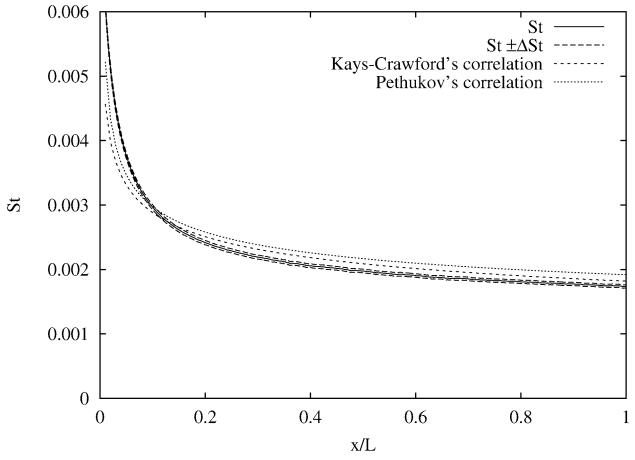

Fig. 10. Heated flat plate: Stanton number.

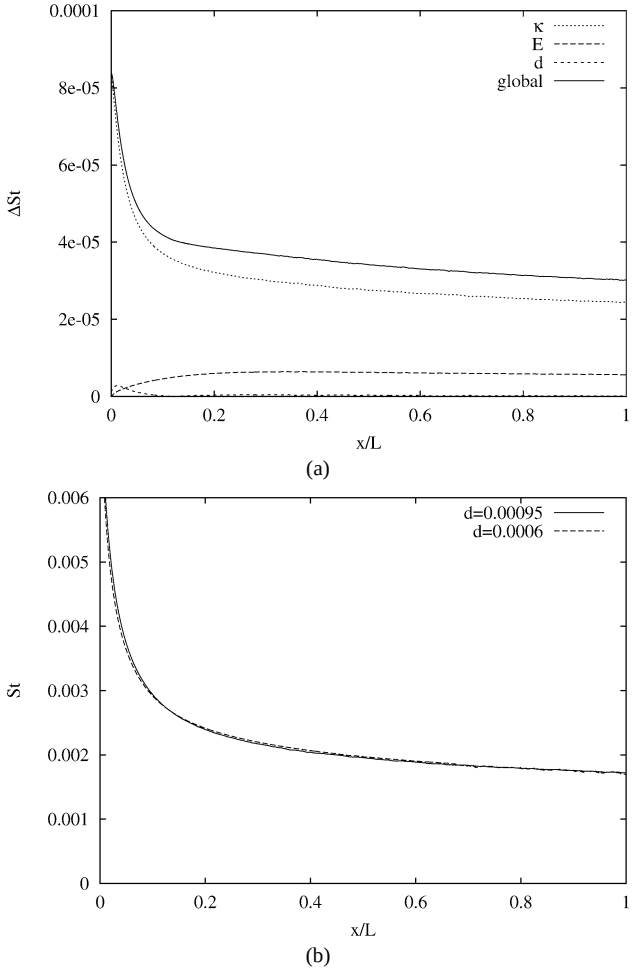

Fig. 11. Heated flat plate: uncertainties in *St* and effect of d on *St*. (a) Uncertainty contributions to the St; (b) Effect of d on *St*.

this flow. Fig. 11(a) presents the contributions of each coefficients to the Stanton number uncertainty. In the present case, the Kármán constant is the main contributor to the total uncertainty. The contribution of the roughness parameter E is about 4 times smaller than that of κ, whereas the distance

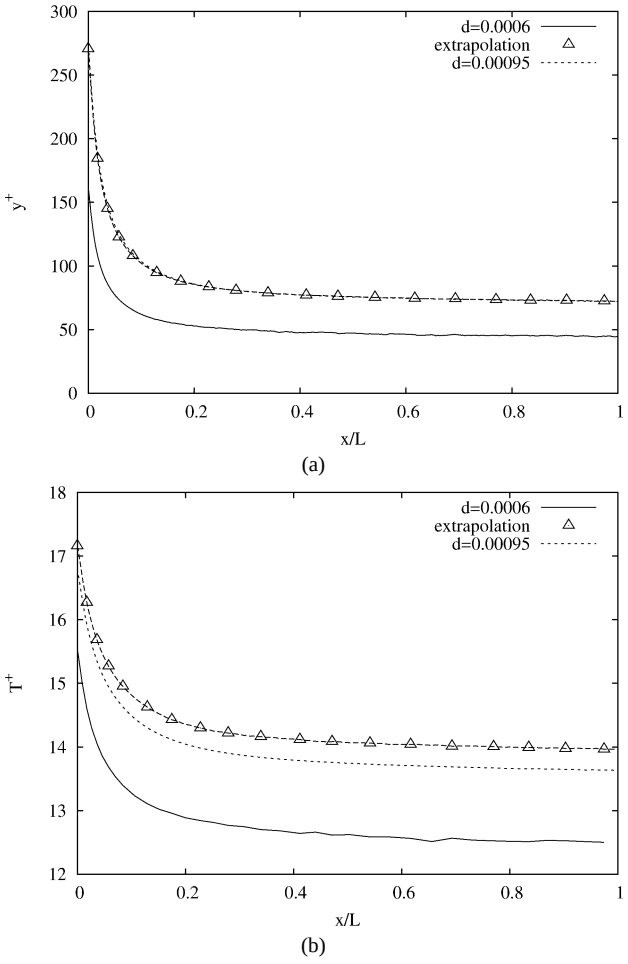

Fig. 12. Flat plate: Effect of d on y^+ and T^+. (a) y^+; (b) T^+.

d to the wall has a negligible effect, except near the leading edge.

Even if the influence of the distance d seems negligible, this parameter is especially interesting to study because its value is not well defined since it is specified by the user. Indeed, there is no textbook approach for its *a priori* determination. The user must perform an *a posteriori* verification of the correctness of his choice. Sensitivity analysis provides quantitative information on how critical the value of d is to the CFD output. In the present case, $\frac{\partial St}{\partial d}$ is small along the wall indicating that the choice of d is not crucial: *St* is virtually insensitive to d except near the leading edge, as shown on Fig. 11(a). To verify this, we follow Turgeon et al. [3] and compare the results of two simulations for $d = 0.00096$ and $d = 0.0006$. Fig. 11(b) shows that the predictions of the Stanton number for the two values of d are identical confirming the trend predicted by $\frac{\partial St}{\partial d}\Delta d$ on Fig. 11: d has no effect on *St* if it is chosen so that y^+ is between 30 and 300.

Fig. 12 shows the effects of d on the distributions of y^+ and T^+. While changes in d do not affect the Stanton number, they have a pronounced effect on both y^+ and T^+. This figure also provides information on the accuracy of the Taylor series approach for fast evaluation of y^+ and T^+ at

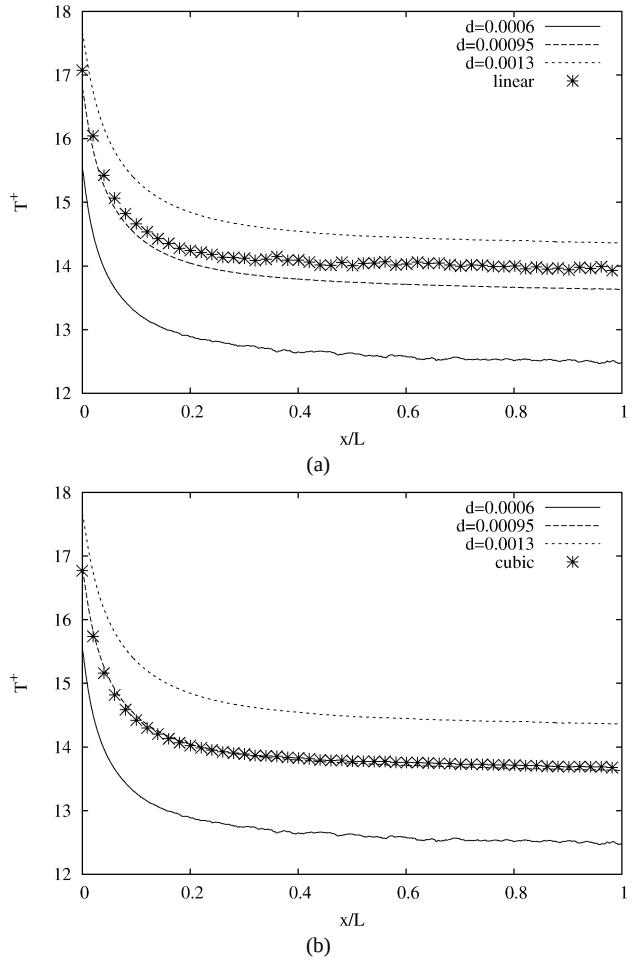

Fig. 13. Flat plate: Fast evaluation of $T^+(d)$. (a) Linear extrapolation; (b) Cubic extrapolation.

nearby values of d. The baseline solution and its sensitivities were obtained for $d = 0.0006$ and are plotted as solid lines. This information is used to obtain Taylor series estimates of y^+ and T^+ at $d = 0.00095$. This represents a perturbation of 0.00035 or 58% from the baseline value. Hence, this constitutes an extreme test for the linear Taylor series approach. The true solution is plotted as a dotted line while Taylor estimates are represented by the triangular symbols. Estimates of y^+ are excellent confirming the linear relationship between y^+ and d (Eq. (7)) even though other terms may implicitly depend on d. However, the linear extrapolation estimate of T^+ is poor confirming the nonlinear dependence of T^+ on d (Eq. (18)).

It is possible to achieve further improvements in the accuracy if one is willing to perform two flow and sensitivity solves for two distinct values of the parameter. It is then possible to use Hermite polynomials to evaluate the flow response at intermediate values of the parameter. For example, we use T^+ as a response variable and the following two values of d:

$d_1 = 0.0006$

$d_2 = 0.0013$

to evaluate the distribution of T^+ at $d = 0.0095$. We use the following form of the Hermite polynomials (Eq. (31)):

$$T^+(x;d) = T^+(x;d_1)\psi_1(\xi) + \frac{\partial T^+}{\partial d}(x;a_1)\psi_2(\xi) + T^+(x,y;d_2)\psi_3(\xi) + \frac{\partial T^+}{\partial d}(x;d_2)\psi_4(\xi)$$

Fig. 13 illustrates the results. Improvements are achieved for two reasons: Δd is smaller and we use higher order polynomials. For completeness, we also show the result from averaging the linear Taylor extrapolations from the two baseline solutions ($d = 0.0006$ and $d = 0.0013$). While the linear prediction is improved over the previous one point Taylor extrapolation, its accuracy is at best fair. The cubic Hermite approximation is surprisingly accurate.

8. Conclusions

A general methodology was applied to perform sensitivity analysis of turbulent flows with heat transfer modeled by the k–ε model of turbulence with wall functions. An adaptive finite element method was used to ensure that flow and sensitivity predictions are grid converged (i.e., producing verified CFD predictions in the sense of Roache [19]). This ensures that discrepancies between predictions and measurements are only due to turbulence modeling and not to numerical inaccuracies. Sensitivity analysis provides useful information for CFD analysts and turbulence modelers. The ability to identify key parameters controlling the flow can help designers focus their attention on the essential aspects of their work. Fast evaluation of nearby flows will prove helpful in answering questions of the type *what happens if we change this or that*. Finally, uncertainty estimates for turbulent flow simulations put CFD on par with experiments which have provided uncertainty bars for many years. Grid converged predictions with uncertainty estimates provide a rigorous framework for comparing predictions and measurements (i.e., validation of CFD predictions in the sense of Roache [19]).

The methodology was verified on a problem possessing an closed form solution (a turbulent heated shear layer). Sensitivity analysis of the backward facing step problem has shown that C_1 and C_2 have the most pronounced effect on the turbulence model and heat transfer predictions. Furthermore, the observed discrepancies between predictions and experimental measurements cannot be explained by uncertainties in the closure coefficients.

For the flat plate problem, the Stanton number is slightly is under-predicted by the k–ε turbulence model with wall functions. Sensitivity analysis confirm the anticipated negligible effect of the wall distance d (user specified wall function data) on the Stanton number provided that d lies in its range of validity ($^+$ between 30 and 300).

Finally sensitivities were used with linear Taylor series and Hermite polynomial for fast evaluation of nearby flows.

The accuracy of this approach was verified by comparing these inexpensive predictions with a full flow solution at the perturbed values of the parameters.

Sensitivity analysis is powerful tool to identify the contribution of each parameter on the flow and thermal response of the system. This provides quantitative feedback for model refinement or for performing better experiments.

Acknowledgements

This work was sponsored in part by NSERC (Government of Canada), FQRNT (Government of Québec), the Canada Research Chair program, and by the Air Force Office of Scientific Research under grants AFOSR F49620-00-1-0299.

References

[1] E. Colin, S. Etienne, D. Pelletier, J. Borggaard, A general sensitivity equation formulation for turbulent heat transfer, in: 36th AIAA Thermophysics Conference, Orlando, FL, June 2003, AIAA Paper 2003-3636.

[2] É. Turgeon, D. Pelletier, J. Borggaard, Sensitivity and uncertainty analysis for variable property flows, in: 39th AIAA Aerospace Sciences Meeting and Exhibit, Reno, NV, January 2001, AIAA Paper 2001-0139.

[3] É. Turgeon, D. Pelletier, J. Borggaard, Application of a sensitivity equation method to the k–ε model of turbulence, in: 15th AIAA Computational Fluid Dynamics Conference, Anaheim, CA, June 2001, AIAA Paper 2001-2534.

[4] É. Turgeon, D. Pelletier, S. Etienne, Sensitivity and uncertainty analysis for turbulent flows, in: 40th AIAA Aerospace Sciences Meeting and Exhibit, Reno, NV, January 2002, AIAA Paper 2002-0985.

[5] J. Borggaard, D. Pelletier, É. Turgeon, A study of optimal cooling strategies in thermal processes, in: 38th AIAA Aerospace Sciences Meeting and Exhibit, Reno, NV, January 2000, AIAA Paper 2000-0563.

[6] M. Putko, P. Newman, A. Taylor, L. Green, Approach for uncertainty propagation and robust design in CFD using sensitivity derivatives, in: 15th AIAA Computational Fluid Dynamics Conference, Anaheim, CA, June 2001, AIAA Paper 2001-2528.

[7] B.E. Launder, J. Spalding, The numerical computation of turbulent flows, Comput. Methods Appl. Mech. Engrg. (1974) 269–289.

[8] F. Ilinca, Méthodes d'éléments finis adaptatives pour les écoulements turbulents, PhD thesis, École Polytechnique de Montréal, 1996.

[9] F. Ilinca, D. Pelletier, Positivity preservation and adaptive solution for the k–ε model of turbulence, AIAA J. 36 (1) (1998) 44–51.

[10] J.P. Chabard, Project N3S de mécanique des fluides—Manuel théorique de la version 3, Tech. Rep. EDF HE-41/91.30B, Électricité de France, 1991.

[11] L. Ignat, D. Pelletier, F. Ilinca, Adaptive computation of turbulent forced convection, Numer. Heat Transfer A 34 (1998) 847–871.

[12] V. Arpaci, P. Larsen, Convection Heat Transfer, Prentice-Hall, Englewood Cliffs, NJ, 1984.

[13] O.C. Zienkiewicz, J.Z. Zhu, The Superconvergent patch recovery and a posteriori error estimates. Part 1: The recovery technique, Internat. J. Numer. Methods Engrg. 33 (1992) 1331–1364.

[14] O.C. Zienkiewicz, J.Z. Zhu, The superconvergent patch recovery and a posteriori error estimates. Part 2: Error estimates and adaptivity, Internat. J. Numer. Methods Engrg. 33 (1992) 1365–1382.

[15] M. Kleiber, T. Hien, The Stochastic Finite Element Method, Wiley, Chichester, 1992.

[16] T. Fadale, Uncertainty Analysis using stochastic finite elements, PhD thesis, University of Washington, 1993.

[17] É. Turgeon, D. Pelletier, J. Borggaard, A general continuous sensitivity equation formulation for complex flows, in: 8th IAA/NASA/USAF/ISSMO Symposium on Multidisciplinary Analysis and Optimization, Long Beach, CA, September 2000, AIAA Paper 2000-4732.

[18] É. Turgeon, D. Pelletier, J. Borggaard, A continuous sensitivity equation method for flows with temperature dependent properties, in: 8th AIAA/NASA/USAF/ISSMO Symposium on Multidisciplinary Analysis and Optimization, Long Beach, CA, September 2000, AIAA Paper 2000-4821.

[19] P.J. Roache, Verification and Validation in Computational Science and Engineering, Hermosa, Albuquerque, NM, 1998.

[20] E. Colin, Analyse de sensibilité de transfert de chaleur turbulent, Master's thesis, École Polytechnique de Montréal, August 2003.

[21] É. Turgeon, D. Pelletier, J. Borggaard, A general continuous sensitivity equation formulation for the k–ε model of turbulence, in: 31st AIAA Fluid Dynamics Conferenceand Exhibit, Anaheim, CA, June 2001, AIAA Paper 2001-3000.

[22] J.C. Vogel, J.K. Eaton, Heat transfer and fluid mechanics measurements in the turbulent reattaching flow behind a backward-facing step, Tech. Rep., Thermosciences Division, Department of Mechanical Engineering, Stanford University, Stanford, CA, August 1984.

[23] H.I. Abu-Mulaweh, B.F. Armaly, T. Chen, Turbulent mixed convection over a backward-facing step, Internat. J. Heat Mass Transfer 44 (14) (2001) 2661–2669.

[24] H.I. Abu-Mulaweh, T. Chen, B.F. Armaly, Turbulent mixed convection flow over a backward-facing step—the effects of the step height, Internat. J. Heat Fluid Flow 23 (6) (2002) 758–765.

[25] H.I. Abu-Mulaweh, T. Chen, B.F. Armaly, Turbulent natural convection flow over a backward-facing step, Experimental Heat Transfer 12 (4) (1999) 295–308.

[26] E. Colin, S. Etienne, D. Pelletier, Application of a sensitivity equation method to turbulent flows with heat transfer, in: 42nd AIAA Aerospace Sciences Meeting and Exhibit, Reno, NV, January 2004, AIAA Paper 2004-1290.

[27] B.E. Launder, Current capabilities for modelling turbulence in industrial flows, Appl. Sci. Res. 48 (1991) 247–269.

[28] D. Lacasse, É. Turgeon, D. Pelletier, Prediction of turbulent separated flow in a turnaround duct using wall functions and adaptivity, Internat. J. Comput. Fluid Dynamics 15 (2001) 209–225.

[29] D. Lacasse, É. Turgeon, D. Pelletier, On the judicious use of the k–ε model, wall functions and adaptivity, Internat. J. Thermal Sci. 43 (2004) 925–938.

[30] W. Kays, M. Crawford, Convective Heat and Mass Transfer, third ed., McGraw-Hill, New York, 1993.